

The radio continuum spectrum of Mira A and Mira B up to submillimeter wavelengths

P. Planesas, J. Alcolea, and R. Bachiller

Observatorio Astronómico Nacional (OAN-IGN), Alfonso XII 3, 28014 Madrid, Spain
e-mail: p.planesas@oan.es

Received 25 November 2015 / Accepted 20 December 2015

ABSTRACT

Aims. We present new measurements of the flux densities at submillimeter wavelengths based on ALMA band 7 (338 GHz, $\lambda 0.89$ mm) and band 9 (679 GHz, $\lambda 0.44$ mm) observations to better constrain the origin of the continuum emission of the Mira AB binary system and to check its orbit.

Methods. We have measured the Mira A and Mira B continuum in ALMA band 7, with a resolution of $\sim 0''.31$, and for the first time in ALMA band 9, with a resolution of $\sim 0''.18$. We have resolved the binary system at both bands, and derived the continuum spectral index of the stars and their relative position. We also analyzed ALMA Science Verification data obtained in bands 6 and 3. Measurements at centimeter wavelengths obtained by other authors have been included in our study of the spectral energy distribution of the Mira components.

Results. The Mira A continuum emission has a spectral index of 1.98 ± 0.04 extending from submillimeter down to centimeter wavelengths. The spectral index of the Mira B continuum emission is 1.93 ± 0.06 at wavelengths ranging from submillimeter to ~ 3.1 mm, and a shallower spectral index of 1.22 ± 0.09 at longer wavelengths. The high precision relative positions of the A and B components are shown to significantly depart from the current (preliminary) orbit by ~ 14 mas.

Conclusions. The Mira A continuum emission up to submillimeter wavelengths is consistent with that of a radio photosphere surrounding the evolved star for which models predict a spectral index close to 2. The Mira B continuum emission cannot be described with a single ionized component. An extremely compact and dense region around the star can produce the nearly thermal continuum measured in the range $\lambda 0.4$ – 3.1 mm, and an inhomogeneous, less dense, and slightly larger ionized envelope could be responsible for the emission at longer wavelengths. Our results illustrate the potential of ALMA for high precision astrometry of binary systems. We have found a significant discrepancy between the ALMA measurements and the predicted orbit positions.

Key words. binaries: general – stars: AGB and post-AGB – stars: atmospheres – stars: individual: Mira A – stars: individual: Mira B

1. Introduction

Mira A (*α* Ceti) is one of the best known stars in the sky. It is the archetype of the long-period variables (LPVs), which are cool, pulsating, mass-losing giants on the asymptotic giant branch (AGB). The spectral type is M5-9IIIe+DA (Skiff 2014). Mira A is one of the nearest LVPs and its circumstellar envelope is one of the brightest in the mm-wave CO lines (e.g., Planesas et al. 1990a,b). Its distance has been determined using different methods, such as the Mira period-luminosity relation (107 ± 12 pc, Knapp et al. 2003), the oxygen-rich Mira period-luminosity relation (115 ± 7 pc, Whitelock et al. 2008), the oxygen-rich Mira period-color-luminosity relation (105 ± 7 pc, Feast et al. 1989), and the HIPARCOS parallax (92 ± 11 pc), which is likely the least reliable method because the star size is three times larger than the measured parallax. In this paper, we adopt a distance to Mira of 110 pc.

Mira A has a companion (Mira B, VZ Ceti), which is itself a variable star and likely to be a white dwarf (Sokoloski & Bildsten 2010) although its nature is still controversial (cf. Ireland et al. 2007). This companion orbits well within the circumstellar envelope of Mira A and accretes gas from the giant. Since the visual confirmation of Mira B discovery (Aitken 1923), its position relative to the primary has been measured to determine the orbit with little success. The latest orbit

parameters can at best be considered preliminary (Prieur et al. 2002). The current separation on the sky is $0''.5$.

In the continuum, the binary system has been resolved with high-resolution observations at several wavelengths: UV and optical with the *Hubble* Space Telescope (HST; Karovska et al. 1997), X-rays with *Chandra* (Karovska et al. 2005), infrared (8 – 18 μ m) with aperture-masking (Ireland et al. 2007), and radio, at cm wavelengths with the VLA (Matthews & Karovska 2006), and very recently at mm wavelengths with JVLA and ALMA (Matthews et al. 2015; Vlemmings et al. 2015). In the last two papers, the radio continuum emission of Mira A at mm wavelengths has been resolved and interpreted as arising in a nonuniform radio photosphere. The Mira B continuum at mm wavelengths has been detected but not resolved and is more than one order of magnitude weaker than that of Mira A. The Mira B continuum is interpreted as arising in a circumstellar hypercompact HII region (Matthews et al. 2015) or a partially ionized wind (Vlemmings et al. 2015).

In spite of the fact that previous authors have analyzed basically the same data (ALMA Science Verification; ALMA Partnership et al. 2015), the values they obtain for the mm-wave spectral index for both stars disagree. Vlemmings et al. (2015) obtain a value of 1.54 ± 0.04 , and from the Matthews et al. (2015) results a value of 1.77 ± 0.10 is obtained for Mira A, which is close to the index of 1.86 predicted by radio photosphere models

(Reid & Menten 1997). For the mm wavelength spectral index of Mira B, the results are 1.72 ± 0.11 (Vlemmings et al. 2015) and 1.45 ± 0.10 (Matthews et al. 2015), both far from the spectral index of 2 expected for an optically thick ionized region.

In this paper, we present the results of radio continuum measurements carried out with ALMA in the submillimeter bands 7 and 9, which are analyzed together with the high angular resolution ALMA Science Verification data obtained in bands 3 and 6, and complemented by cm wavelength results obtained by other authors. Our goal is to study the cm-to-submm radio continuum spectrum of Mira A and B to better constrain the origin of the continuum emission in each star. The potential of ALMA for high precision astrometry of nearby wide binary systems is also discussed.

2. Observations

We performed ALMA radio continuum observations of the Mira system in band 9 at 679.0 GHz on 2014 June 16 via an array configuration of 33 antennas with baselines up to 650 m. The angular resolution was $0''.21 \times 0''.15$. The continuum bandwidth was 7.95 GHz wide, composed of four 2 GHz wide contiguous basebands. The system temperature was 1070 K. Bandpass and phase calibration was performed pointing to the quasars J2253+1608 and J0217+0144, respectively. Flux density calibration was performed with the quasar J2258-279, assuming a flux density of 0.217 Jy. Uranus was used as the primary flux scale calibrator to determine the flux density of the quasar in bands 3 and 7, which was extrapolated to band 9 following the standard procedure described in the ALMA Technical Handbook, where it is claimed that an accuracy better than 15% is achieved. As there is no guarantee that the spectral index is linear up to band 9, we assume a conservative accuracy of $\sim 20\%$ for the absolute flux scale.

ALMA radio continuum observations in band 7 at 338.3 GHz were performed on 2014 June 12, 14, and 15 using an array configuration of 34 antennas with baselines up to 650 m. The angular resolution was $0''.32 \times 0''.30$. Two 2 GHz wide basebands, centered at 332.0 and 344.6 GHz, were used for the continuum measurements. Bandpass and phase calibration was performed pointing to J0224+0659 (J0423-0120 on June 14) and J0217+0144, respectively. Flux density calibration was performed with different quasars on the different dates. The average flux density obtained for J0217+0144, the phase calibrator common in all three runs, was 0.344 ± 0.024 Jy; the uncertainty of 7% reflected the different values obtained in the observation spectral windows and the three runs. This proves the consistency of the ALMA flux calibration in band 7 and provides a measure of the uncertainty in the measured fluxes due to the calibration transfer to secondary calibrators, which is in agreement with the systematic flux uncertainty in band 7 of less than 10% claimed by ALMA (e.g., Fomalont et al. 2014). On June 12 the data were taken with average atmospheric conditions (~ 1.0 mm of precipitable water vapor; pwv), leading to a higher noise level than the data taken on June 14 and 15 at very good conditions (~ 0.6 mm of pwv). We only had to perform minor manual flagging during the calibration step.

Band 7 and band 9 observations correspond to our Cycle 1 project 2012.1.00047.S. The phase of Mira A was ~ 0.1 during the observations. Band 3 and band 6 observations correspond to the ALMA-led, long baseline Science Verification campaign (ALMA Partnership et al. 2015) obtained in 2014 October and November and described elsewhere (Matthews et al. 2015; Vlemmings et al. 2015). The observing frequency in band 3

was 94.2 GHz and the synthesized beam was $0''.070 \times 0''.060$ with a position angle (PA) of the major beam axis of $76^\circ.6$, counted from the north to the east. In band 6, the observing frequency was 229.6 GHz and the synthesized beam was $0''.0344 \times 0''.0241$ with PA = $19^\circ.2$. The Mira A phase was ~ 0.5 during this Science Verification observing period.

3. Data reduction

A first look at the band 9 data revealed the strong continuum source Mira A and an order of magnitude weaker secondary companion Mira B. The ALMA continuum spectrum consisted of 512 13.8 km s^{-1} wide channels where many spectral lines appear. We cleaned the maps corresponding to the channels free of line emission and also excluded the end channels of each spectral window. The data processing was performed with the CASA package and we used a Briggs robust value of 0.5 for cleaning. The rms noise in the original cleaned image was 13 mJy beam^{-1} , which is an order of magnitude higher than expected for a 219-second integration time. The self-calibration on the strong continuum source reduced the noise to $1.9 \text{ mJy beam}^{-1}$ ($S/N > 700$), after the primary beam correction was applied to produce the final image. The synthesized beam was $0''.213 \times 0''.149$ with a position angle of $56^\circ.9$.

The images of Mira A and B (see Fig. 1, top panel) appear clearly separated in the final band 9 image. We performed a simultaneous two-dimensional Gaussian fit to determine the flux and size of each source. The total flux is $1460.8 \pm 0.5 \text{ mJy}$ for Mira A and $124.8 \pm 0.5 \text{ mJy}$ for Mira B. The quoted value for the flux uncertainty is the formal error in the Gaussian fit, and this does not include the uncertainty in the absolute flux density calibration, which is much larger. The total flux corresponding to the emission area around each star is 1458 mJy for Mira A and 123 mJy for Mira B, in agreement with the previous values. Mira B is not resolved, within uncertainties. The convolved size of Mira A is slightly larger than the restored beam. A rough estimate of the deconvolved size of the photosphere of Mira A, assumed to be a uniform intensity disk, is $\sim 0''.065 \pm 0''.006$. The higher resolution observations of the band 6 Science Verification observations have provided a much more precise value of $0''.042 \pm 0''.002$.

Two spectral windows of 128 channels 27.2 km s^{-1} wide were used for the band 7 continuum measurements centered at rest frequencies of 332.0 and 344.6 GHz. The imaging procedure was similar to that of band 9 data: We only cleaned the line free channels, excluded the end channels of each spectral window, applied self-calibration, and cleaned with a Briggs robust value of 0.5. The fitted beam used in restoration was $0''.316 \times 0''.304$ at PA = $37^\circ.9$. The final image noise was $0.20 \text{ mJy beam}^{-1}$ ($S/N > 1500$).

The image of Mira B in band 7 (see Fig. 1, second panel) appears partially overlaid with that of Mira A, therefore, a simultaneous two-dimensional Gaussian fit is required to determine the flux of each source. Both sources are unresolved. The total flux is $346.64 \pm 0.1 \text{ mJy}$ for Mira A and $25.5 \pm 0.2 \text{ mJy}$ for Mira B. The same comment on the uncertainties for band 9 also applies here. The total fluxes, which we estimated by defining the two emission areas with polygons, produced very similar results (cf. Table 1).

Our results from measurements made in mid-June 2014 disagree with the observations of Ramstedt et al. (2014) carried out in October 2013 with ACA and in February and May 2014 with the main array. These observations obtained flux values roughly 30% smaller than ours, namely 252.3 mJy for Mira A

Table 1. Continuum flux density of Mira A and Mira B measured with ALMA.

Band	Frequency (GHz)	Epoch	Mira A		Mira B		
			Phase	S_ν (mJy)	S_ν (mJy)	S_ν (mJy)	
9	678.96	2014-06-16	0.11	Gaussian fit 1460.8 ± 0.5	Polygon 1458	Gaussian fit 124.8 ± 0.5	Polygon 123
7	338.27	2014-06-12	0.09	346.4 ± 0.1	~ 347	25.5 ± 0.2	~ 26
6	229.55	2014-10-29	0.51	152.0 ± 0.2	149.7	11.29 ± 0.02	11.0
3	94.19	2014-10-17	0.48	33.48 ± 0.01	33.5	2.58 ± 0.01	2.1

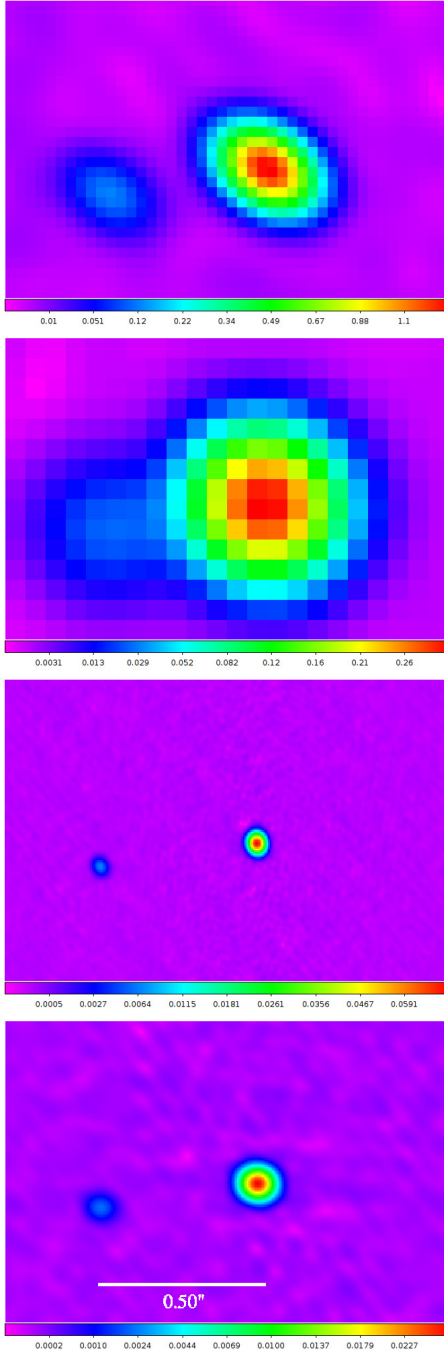


Fig. 1. Continuum images of the Mira AB binary at the ALMA bands 9, 7, 6, and 3 (from top to bottom). The size of the images is $1''.32 \times 0''.90$. A square root scale has been selected for the intensity in all frames. The corresponding flux scale is shown at the bottom of each panel.

and 15.3 mJy for Mira B. They obtained these values from an image made via the emission free channels from the spectral

windows used to map the CO (3–2) emission. The resulting continuum image, taken with an angular resolution of $\sim 0''.5$, was marginally resolved, but the emission corresponding to the two components was not separated in the map. The possible variability of the emission cannot explain the different results because the measurements with the main array were taken a few months apart. Moreover, [Ramstedt et al. \(2014\)](#) do not mention any change in the emission in their three epoch observations, during which the phase changed from 0.33 to 0.97. Despite the reason for disagreement, we later see that their flux values do not agree with the overall shape of the continuum spectrum of both stars.

We have not calibrated the band 6 and band 3 data obtained in the Science Verification campaign again, as these data have been carefully calibrated by other authors (see the comparison of different results in [Matthews et al. 2015](#)). Instead, we have obtained the flux density from the images provided by the ALMA Partnership (2015), both by fitting a Gaussian function to and by computing the flux in an area corresponding to the emission from each star. The results obtained with the two methods agree; cf. Table 1. The total flux values obtained for Mira A and B in band 6 by Gaussian fitting are 152.0 mJy and 11.3 mJy, respectively, and 33.5 mJy and 2.58 mJy in band 3. As expected, these results agree very well with those previously obtained by [Vlemmings et al. \(2015\)](#) and [Matthews et al. \(2015\)](#).

The results of our analysis are summarized in Table 1. The values obtained with two methods (Gaussian fit, and total flux within a polygon surrounding the emitting area) agree in all bands.

4. The shape and origin of the continuum spectra

The radio continuum spectra for Mira A and Mira B are shown in Fig. 2, which includes the results obtained from ALMA data presented in this paper (black triangles), from recent papers ([Ramstedt et al. 2014](#); [Matthews et al. 2015](#); [Vlemmings et al. 2015](#)), and from previous VLA data, specifically, the weighted average of measurements made at 8.5 and 22.5 GHz by [Matthews & Karovska \(2006\)](#) and the Mira A measurements at 43.1 GHz by [Reid & Menten \(2007\)](#).

The black line is the fit to all the Mira A measurements, which is well represented by a power law with a spectral index of $\alpha = 1.98 \pm 0.04$. Errors in the absolute calibration within the estimated uncertainty would not significantly change this value. For example, a reduction of 20% in the band 9 flux value due to a hypothetical overestimation in the absolute calibration would barely reduce the spectral index to $\alpha = 1.96 \pm 0.04$. If a thermal spectrum is assumed, then it can be described as $S_{\nu,A} = (31.0 \pm 0.6) (\nu/100 \text{ GHz})^2$ mJy. The cyan dashed line shows the result of fitting the [Matthews et al. \(2015\)](#) data with the $\nu^{1.86}$ law predicted by the radio photosphere model of [Reid & Menten \(2007\)](#) for the centimeter wavelength range, which clearly deviates from the full continuum spectrum at the low frequency range and, possibly, at the submillimeter frequencies as

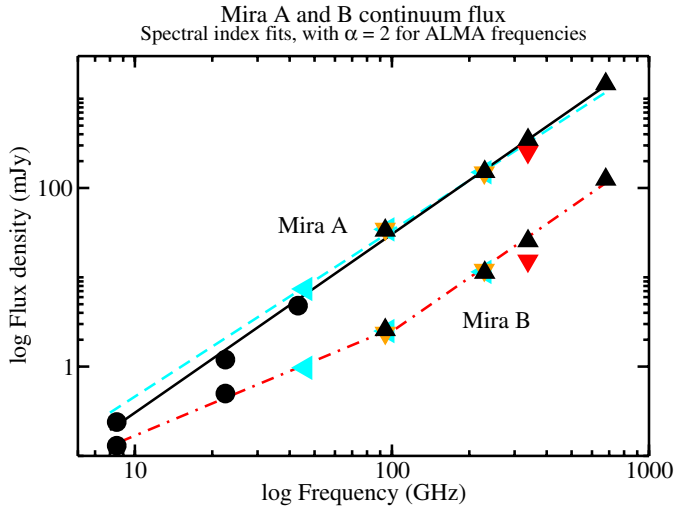


Fig. 2. Measured values of the Mira A and Mira B continuum flux. Black upward facing triangles correspond to the ALMA measurements presented here. Orange downward facing triangles correspond to the results obtained from ALMA data by Vlemmings et al. (2015), and red downward facing triangles to those from Ramstedt et al. (2014). Cyan leftward facing triangles correspond to the results obtained from ALMA and JVA data by Matthews et al. (2015). Black circles correspond to VLA results extracted from the papers by Matthews & Karovska (2006) and Reid & Menten (2007). The straight lines correspond to fits to all or to a fraction of the data obtained toward each star.

well. On the other hand, Reid & Menten (2007) performed radiative transfer calculations for frequencies up to 10 THz ($\lambda 30 \mu\text{m}$) and concluded that the spectral index remains close to 2, although not all the opacity contributions were considered in the model. In conclusion, the emission of Mira A detected with ALMA seems to arise mainly from the radio photosphere, but in the submm range additional minor contributions to the flux might exist, such as a small contribution of warm dust in the dust shell around the star.

The continuum spectrum of Mira B cannot be described by a single power law, as shown by the dash-dotted red lines in Fig. 2. At frequencies below ~ 95 GHz, the spectrum can be described as $S_{\nu,B} = (2.65 \pm 0.06) (\nu/100 \text{ GHz})^{1.22 \pm 0.09}$ mJy. At frequencies higher than ~ 95 GHz, the spectrum is best described by a power 2 law. In fact, the fit to the results obtained at frequencies in the range 94 to 680 GHz, discarding the value at 338 GHz, which lies clearly below the straight line and yields a spectral index of $\alpha = 1.93 \pm 0.06$. If a thermal spectrum is assumed for the high frequency range, it can be described as $S_{\nu,B} = (2.66 \pm 0.05) (\nu/100 \text{ GHz})^2$ mJy. Matthews et al. (2015) already showed that the flux density measured in ALMA bands 6 and 7 are well above the values that were expected from the continuum spectrum below 100 GHz, and concluded that free-free emission from a hypercompact HII region (HCHII) cannot describe the full continuum spectrum. Our observations show that the trend extends to higher frequencies, therefore, the change in spectral index is not apparent, but reflects the complexity of the environment that surrounds Mira B; this star is embedded in the highly structured Mira A envelope (Ramstedt et al. 2014), accreting matter through a circumstellar disk.

A two-component model may be needed to explain Mira B continuum spectrum. The coefficient of the fit of the high frequency ($\nu > 90$ GHz) part of the spectrum to a thermal law can be used to determine the size of the emitting region under the assumption of optically thick emission (ν^2 law) and a typical

electron temperature of 10^4 K. From the fit, we derive a half power angular size of a Gaussian distribution of $0''.019$, which corresponds to 3.1×10^{13} cm at a distance of 110 pc. If the distribution is better represented by an uniform disk, then the corresponding disk size is 4.6×10^{13} cm. These values agree with the size of $\sim 4 \times 10^{13}$ cm estimated by Matthews et al. (2015) based solely in band 6 measurements, and the size of 4.3×10^{13} cm derived by Vlemmings et al. (2015). The turnover frequency of the continuum emission is clearly larger than 700 GHz, therefore, the average electron density (in fact, $\sqrt{\langle N_e^2 \rangle}$) must be larger than $5 \times 10^8 \text{ cm}^{-3}$. This value is 2–3 orders of magnitude larger than the typical density in a HCHII region (Kurtz 2005).

The continuum flux density of the lowest frequency range ($\nu < 90$ GHz) has a spectral index that is not as steep, although the index is not as low as that of an ionized wind (e.g., Báez-Rubio et al. 2013). The continuum emission may originate in a region more extended than the region responsible for the thermal emission. A hyper-compact HII region, with a nonuniform gas density, density gradients, or clumpy structure can produce a continuum spectrum with a spectral index $\alpha \sim 1.2$ (Franco et al. 2000). As an example, this spectral index can be produced in a nebula with a power-law density distribution like $N_e \propto r^{-3.2}$ (Olson 1975; Panagia & Felli 1975). The turnover frequency for the ionized component responsible for the low frequency part of the continuum spectrum is larger than 50 GHz, therefore, the emission measure exceeds $10^{10} \text{ pc cm}^{-6}$. However, the Lyman continuum necessary to ionize a region like this cannot be provided solely by the white dwarf emission owing to its low effective temperature of < 17000 K (Reimers & Cassatella 1985). The accretion-power luminosity is likely to be the main source of ionizing photons.

We can obtain rough limit estimates of the ionized region characteristics by assuming that the total luminosity of $10^{33} \text{ erg s}^{-1}$ of Mira B (Sokoloski & Bildsten 2010) is an upper limit to the energy emitted in Lyman continuum photons. The upper limit of the ionizing photons' rate and the lower limit of the emission measure, taken together, imply an upper limit for the ionized region size of 1.2×10^{14} cm and a lower limit for the density of $1.6 \times 10^7 \text{ cm}^{-3}$. These parameters describe a region that is slightly larger and less dense than the inner region, where the thermal continuum measured in the 3 to 0.4 mm wavelength range originates. In fact, its size is comparable to that of the accretion disk as determined by Ireland et al. (2007). In spite of all the quantitative uncertainties, we conclude that a small ionization-limited envelope with density gradients or winds, which explain the shallow spectral index at cm-wavelength frequencies, surrounds an extremely compact and dense inner region that emits a nearly thermal spectrum.

5. Relative positions of the binary system

The astrometric measurements carried out with ALMA can be useful to study the orbit of the Mira system. In fact, although the relative position of the two stellar components has been measured since the discovery of Mira B, the orbit of the Mira binary system is not yet well determined. The short distance between the stars and the large brightness contrast has made the measurement of their relative positions rather difficult. Before 1980, the period of the computed orbits ranged from 14 to 841 years (cf. Baize 1980). In fact, an examination of the early measurements show a large dispersion. In Fig. 3 we binned the available measurements in five-year intervals to show the average position in each bin and the corresponding 1σ dispersion, which

Table 2. Relative positions of the Mira binary system.

Epoch	$\Delta\alpha \cos \delta$ ''	$\Delta\delta$ ''	ρ ''	θ °	Telescope	Reference
1995.9467	0.549 ± 0.002	-0.182 ± 0.002	0.578	108.3	HST	Karovska et al. (1997)
2004.1295	0.525 ± 0.003	-0.149 ± 0.003	0.546	105.8	HST	Ireland et al. (2007)
2004.1342	0.5281 ± 0.0008	-0.1465 ± 0.0008	0.5480	105.51	HST	This paper
2007.7283	0.5093 ± 0.0020	-0.1258 ± 0.0022	0.5246	103.87	HST	This paper
2014.1478	0.4721 ± 0.0006	-0.0792 ± 0.0007	0.4787	99.53	JVLA	Matthews, priv. comm.
2014.4517	0.4687 ± 0.0006	-0.0750 ± 0.0005	0.4747	99.09	ALMA band 7	This paper
2014.4572	0.4695 ± 0.0003	-0.0752 ± 0.0003	0.4755	99.10	ALMA band 9	This paper
2014.8050	0.46620 ± 0.00011	-0.07119 ± 0.00010	0.47161	98.68	ALMA band 3	This paper
2014.8309	0.46610 ± 0.00007	-0.06980 ± 0.00008	0.47129	98.52	ALMA band 6	This paper

Notes. ρ is the star separation and θ is the position angle. The uncertainties in the offsets are the formal errors in the Gaussian fits.

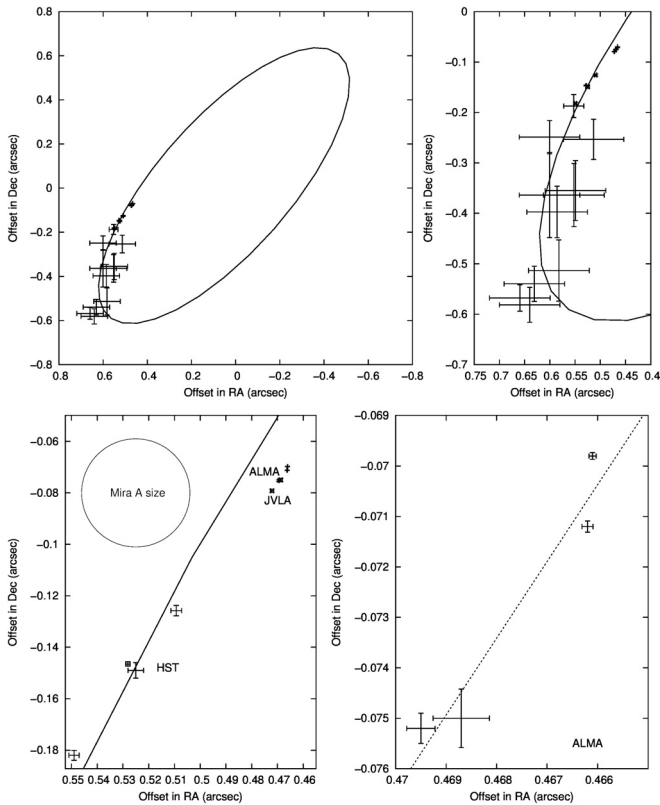


Fig. 3. Relative position of the binary. In the *top panels*, the preliminary orbit determined by Prieur et al. (2002) is overlaid on the results of optical observations done since 1923, binned in five-year intervals. The 1σ dispersion of the values in each bin is shown with error bars. The HST and ALMA results of our analysis are included too, and they are more clearly shown in the *bottom left panel* together with HST and JVLA results by other authors (cf. Table 2). The deviation from the preliminary orbit is distinctly seen. The circle shows the size of Mira A at 229 GHz. The *bottom right panel* shows the ALMA measurements and their formal uncertainty. The dotted line is the result of an unweighted linear fit used to estimate the accuracy of the ALMA derived positions; the rms of the residuals is $0''.0008$.

is typically $0''.06$ in each coordinate. The two components were clearly separated for the first time in 1983 (Karovska et al. 1991), using the new technique of speckle interferometry, which was employed thereafter. A further improvement in the determination of the relative position of the binary was achieved with HST (Karovska et al. 1997). The precision achieved in the determination of the separation of the stars was $\sim 0''.003$.

The ALMA continuum measurements provide further improvement in the precision of the determination of the relative position of the Mira components, down to a fraction of a milliarcsecond. This is the expected positional uncertainty due to the high signal-to-noise ratio of the Mira A and B detections (cf. Eq. (1) in Reid et al. 1988) and the rms of the residuals of a linear fit. This fit is a straight line, representing a very short arc of the orbit, to the positions determined from the ALMA measurements (see bottom right panel in Fig. 3). In Table 2 we list the results of our analysis of the ALMA data together with our own analysis of additional HST archival data (HST projects 10091 and 11224), which are plotted in the bottom panels of Fig. 3. The HST results lie close to the preliminary orbit, but this is not the case for the ALMA results, which clearly lie significantly apart by $\sim 0''.014$. Our results for the ALMA bands 3 and 6 Science Verification data agree with the independent analysis made by Vlemmings et al. (2015), and with the JVLA results obtained by Matthews et al. (2015). Therefore, we have to conclude that either significant structure in the radio emitting area of the binary components causes an apparent offset of their relative position of the centroids with respect to the orbit or the orbit parameters need improvement.

In fact, Mira A radio disk has been resolved using band 6 ALMA data, revealing the presence of a hotspot (Matthews et al. 2015; Vlemmings et al. 2015) slightly off-center (by $\sim 0''.003$) of the star disk, although these authors disagree with the value of the hotspot contribution to the total flux. If the contribution is as large as proposed by Matthews et al. (2015), the location of the emission center of Mira A that would be obtained by fitting a single Gaussian, as we have done, would be wrong by ~ 1.4 mas approximately toward the west. This would apparently shorten, by the same amount, the offset in right ascension (RA) between the binary components. This offset is far too small to account for the discrepancy of $\sim 0''.014$ between the relative positions measured with ALMA and JVLA and the preliminary orbit.

Therefore, we conclude that the orbit needs to be improved taking the new observational results into account. However, this may not be an easy task because the new measurements (and measurements in the decades ahead) correspond to a region of the orbit that is far from the ends of the apparent ellipse, so they are not the most favorable to compute a better orbit.

The Mira AB system is well suited to determine the mass of an AGB star, which is usually an unknown in the studies of long period variables and severely limits the modeling of the star evolution. In fact, a good determination of the distance is available for Mira AB (and a better value may be provided soon by the *Gaia* mission), therefore, the total mass of the system can be kinematically derived from the orbit parameters, if

they are well determined. The mass of Mira B has been estimated to be $\sim 0.6 M_{\odot}$, both under the hypothesis that the star is a white dwarf (Sokoloski & Bildsten 2010) or a low-mass main-sequence star (Ireland et al. 2007). Currently, with the adopted distance of 110 pc and the preliminary orbit computed by Prieur et al. (2002), we obtain $m_A + m_B \simeq 2.7 M_{\odot}$, so $m_A \sim 2 M_{\odot}$, but this value is uncertain as we have shown that the orbit needs to be corrected.

6. Conclusions

We present the results of radio continuum measurements carried out with ALMA in the submillimeter bands 7 and 9, corresponding to frequencies in the submm range of 338 and 679 GHz, respectively. We reduced the data and produced maps, after removing the numerous spectral lines that appear in the observed spectral windows. High angular resolution ALMA Science Verification data obtained in bands 3 and 6 in the mm-wavelength range have also been reduced. The flux determined with ALMA for both Mira components follow a power law of spectral index ~ 2.0 .

The Mira A continuum emission is well described by an optically thick thermal spectrum of spectral index $\alpha = 1.98 \pm 0.04$, which extends from cm-to-submm wavelengths (frequency from 8 to 700 GHz). This is in agreement with radiative transfer models, which conclude that the spectral index of the radio photosphere that surrounds the evolved star remains close to 2 for frequencies up to the THz range (Reid & Menten 2007).

The Mira B continuum spectrum is described with spectral index $\alpha = 1.22 \pm 0.09$ at frequencies below ~ 95 GHz and $\alpha = 1.93 \pm 0.06$ at higher frequencies up to the submm range. Therefore, it cannot be described with a single ionized component. We propose a two-component model, consisting of an extremely compact and dense region around the star than can produce the nearly thermal continuum measured at the high frequency range and, surrounding this region, a slightly larger and less dense, nonuniform ionized envelope with density gradients or winds that are responsible for the emission at longer wavelengths. The ionizing source is likely associated with the accretion process.

The potential of ALMA for high precision astrometry of nearby binary systems has been discussed. In a few minutes of observing time, the positions can be determined with great accuracy for distances up to 100 pc, even in ALMA band 9. The ALMA continuum measurements provide an order of magnitude improvement with respect to HST measurements in the precision of the determination of the relative position of the Mira components down to a tenth of a milliarcsecond. However, because of the extremely high angular resolution of ALMA, which is able to resolve the structure in the stellar disks, some modeling may be required to determine the geometrical center of the disks. Nevertheless, we have found a significant discrepancy, of the

order of $0''.014$, between the ALMA measurements and the predicted orbit. This discrepancy is evidence that the orbit parameters need to be improved taking the high precision results of the current observations into account. Better orbit parameters would help to constrain the Mira A mass and allow us to improve the evolutionary modeling of this AGB star.

Acknowledgements. This paper makes use of the following ALMA data: ADS/JAO.ALMA#2013.1.00047.S. ALMA is a partnership of ESO (representing its member states), NSF (USA), and NINS (Japan) together with NRC (Canada), NSC, and ASIAA (Taiwan) in cooperation with the Republic of Chile. The Joint ALMA Observatory is operated by ESO, AUI/NRAO, and NAOJ. Also, some data is based on observations made with the NASA/ESA *Hubble* Space Telescope, obtained from the data archive at the Space Telescope Science Institute. STScI is operated by the Association of Universities for Research in Astronomy, Inc. under NASA contract NAS 5-26555. This research has been partially funded by the Spanish DGCYT grants FIS2012-32096 and FIS2012-32032, and has received travel funding from the European Commission Seventh Framework Programme (FP/2007-2013) under grant agreement No. 283393 (RadioNet3) through the RadioNet Networking Activity MARCUs (Mobility for ALMA Regional Centre Users). The authors thank Edwige Chapillon and the IRAM ARC node for their assistance in the data calibration, and Lynn Matthews for providing additional information on Fig. 1 in her 2015 paper.

References

- Aitken, R. G. 1923, *PASP*, **35**, 323
 ALMA Partnership, Fomalont, E. B., Vlahakis, C., et al. 2015, *ApJ*, **808**, L1
 Báez-Rubio, A., Martín-Pintado, J., Thum, C., & Planesas, P. 2013, *A&A*, **553**, A45
 Baize, P. 1980, *A&AS*, **39**, 83
 Feast, M. W., Glass, I. S., Whitelock, P. A., & Catchpole, R. M. 1989, *MNRAS*, **241**, 375
 Fomalont, E., van Kempen, T., Kneissl, R., et al. 2014, *The Messenger*, **155**, 19
 Franco, J., Kurtz, S., Hofner, P., et al. 2000, *ApJ*, **542**, L143
 Ireland, M. J., Monnier, J. D., Tuthill, P. G., et al. 2007, *ApJ*, **662**, 651
 Karovska, M., Nisenson, P., Papaliolios, C., & Boyle, R. P. 1991, *ApJ*, **374**, L51
 Karovska, M., Hack, W., Raymond, J., & Guinan, E. 1997, *ApJ*, **482**, L175
 Karovska, M., Schlegel, E., Hack, W., Raymond, J. C., & Wood, B. E. 2005, *ApJ*, **623**, L137
 Knapp, G. R., Pourbaix, D., Platais, I., & Jorissen, A. 2003, *A&A*, **403**, 993
 Kurtz, S. 2005, in *Massive Star Birth: A Crossroads of Astrophysics*, eds. R. Cesaroni, M. Felli, E. Churchwell, & M. Walmsley, *IAU Symp.*, **227**, 111
 Matthews, L. D., & Karovska, M. 2006, *ApJ*, **637**, L49
 Matthews, L. D., Reid, M. J., & Menten, K. M. 2015, *ApJ*, **808**, 36
 Olmon, F. M. 1975, *A&A*, **39**, 217
 Panagia, N., & Felli, M. 1975, *A&A*, **39**, 1
 Planesas, P., Bachiller, R., Martín-Pintado, J., & Bujarrabal, V. 1990a, *ApJ*, **351**, 263
 Planesas, P., Kenney, J. D. P., & Bachiller, R. 1990b, *ApJ*, **364**, L9
 Prieur, J. L., Aristidi, E., Lopez, B., et al. 2002, *ApJS*, **139**, 249
 Ramstedt, S., Mohamed, S., Vlemmings, W. H. T., et al. 2014, *A&A*, **570**, L14
 Reid, M. J., & Menten, K. M. 1997, *ApJ*, **476**, 327
 Reid, M. J., & Menten, K. M. 2007, *ApJ*, **671**, 2068
 Reid, M. J., Schneps, M. H., Moran, J. M., et al. 1988, *ApJ*, **330**, 809
 Reimers, D., & Cassatella, A. 1985, *ApJ*, **297**, 275
 Skiff, B. A. 2014, *VizieR Online Data Catalog*, B/mk
 Sokoloski, J. L., & Bildsten, L. 2010, *ApJ*, **723**, 1188
 Vlemmings, W. H. T., Ramstedt, S., O’Gorman, E., et al. 2015, *A&A*, **577**, L4
 Whitelock, P. A., Feast, M. W., & van Leeuwen, F. 2008, *MNRAS*, **386**, 313